Understanding Aqueous Stability and Filtration Capability of MoS_2 Membranes

Zhongying Wang[a1], Qingsong Tu[a1], Sunxiang Zheng[a], Jeffrey J. Urban[b], Shaofan Li[a], Baoxia Mi[a*]

1. These authors contributed equally to the work.

[a] Department of Civil and Environmental Engineering
University of California
Berkeley, CA 94720

[b] The Molecular Foundry
Lawrence Berkeley National Laboratory
Berkeley, CA 94720

[*] The author to whom correspondence should be addressed.

E-mail: mib@berkeley.edu; Tel.: (510) 664-7446.

ABSTRACT

Membranes made of layer-stacked two-dimensional molybdenum disulfide (MoS_2) nanosheets have recently shown great promise for water filtration. At present, the reported water fluxes vary significantly while the accountable structure and properties of MoS_2 nanochannels are largely unknown. This paper aims to mechanistically relate the performance of MoS_2 membranes to the size of their nanochannels in different hydration states. We discovered that fully hydrated MoS_2 membranes retained a 1.2-nm interlayer spacing (or 0.9-nm free spacing), leading to high water permeability and moderate-to-high ionic/molecular rejection. In comparison, completely dry MoS_2 membranes had a 0.62-nm interlayer spacing (or 0.3-nm free spacing) due to irreversible nanosheet restacking and were almost impermeable to water. Furthermore, we revealed that the interlayer spacing of MoS_2 membranes in aqueous solution is maintained by comparable van der Waals and hydration forces, thereby ensuring the aqueous stability of MoS_2 membranes without the need of crosslinking. In addition, we attributed the high water flux (30-250 L m^{-2} h^{-1} bar^{-1}) of MoS_2 membranes to the low hydraulic resistance of smooth, rigid MoS_2 nanochannels. We also concluded that compaction of MoS_2 membranes with a high pressure helps create a more neatly stacked nanostructure with minimum voids or looseness, leading to stable water flux and separation performance. Besides, this paper systematically compares MoS_2 membranes with the widely studied graphene oxide membranes to highlight the uniqueness and advantages of MoS_2 membranes for water filtration applications.

Keywords: molybdenum disulfide; layer-stacked membrane; interlayer spacing; aqueous stability; water filtration; membrane separation.

Novel restacking of two-dimensional (2D) nanosheets produced *via* exfoliation of bulk inorganic layered materials can lead to layer-stacked laminar membranes that have excellent mechanical and physicochemical properties.[1-5] By fine-tuning the interlayer spacing between neighboring nanosheets, it is possible to achieve high water permeance while rejecting unwanted species.[6] For example, the widely studied layer-stacked graphene oxide (GO) membranes have shown a potential for desalination,[7] water purification,[8-11] oil/water separation[12,13] and anti-fouling coating.[14-16] The unoxidized regions of GO nanosheets provide a nearly frictionless surface for water to flow, promising high water permeability.[17] On the other hand, however, the complete recovery of graphitic regions by removing the oxygenated functional groups unavoidably decreases the interlayer spacing of GO membranes to as low as 0.36 nm, which is close to that in bulk graphite and thus undermines water permeability.[18] Besides, the presence of oxygenated functional groups in GO causes several problems. First, the hydrophilicity of functional groups leads to membrane instability in aqueous environment,[19,20] demanding crosslinking[21] or reduction[8,22] to ensure membrane integrity but inevitably increasing the fabrication complexity and structural heterogeneity. Second, the hydration of oxygenated functional groups increases the interlayer spacing and thus deceases membrane selectivity.[23,24] Third, the existence of surface oxygenated groups could impede the water transport due to their interactions with water molecules *via* hydrogen bond.[25]

The above problems facing the membranes made by layer-stacking GO nanosheets using the weak electrostatic interaction can be potentially circumvented by membranes made by layer-stacking MoS_2 nanosheets using the strong van der Waals structure. First, because MoS_2 does not have any hydrophilic functional groups extruding from its surface, the van der Waals force between MoS_2 nanosheets could potentially dominate and prevent the layer-stacked MoS_2 nanosheets from redispersion in water.[26] Second, the high surface smoothness (due to the lack of crosslinkers or functional groups) of MoS_2 nanosheets may lead to low hydraulic resistance and thus potentially high water flux. Third, the MoS_2 nanosheet is much more rigid out-of-plane than the GO nanosheet thanks to the existence of three atomic layers,[27] leading to a nanostructure that is less likely to be further compacted under pressure,[26] in contrast to the often observed elastic deformation of GO nanochannels.[23] Besides, the chemical and mechanical stability,[28] non-toxicity,[29,30] high surface area,[31] and versatile physicochemical properties[32,33] of MoS_2 nanosheets may enable novel multi-functional membranes with advanced reactivities.[34]

To date, research on layer-stacked MoS_2 membranes for water filtration is just emerging, with exciting behaviors reported but many fundamental questions unanswered.[26,35,36] For example, MoS_2 membrane has demonstrated a water flux of around 245 L h^{-1} m^{-2} bar^{-1} (LMH/bar) in one study,[26] much higher than ~ 45 LMH/bar of a GO membrane with comparable thickness and dye rejection.[37] Additionally, extraordinary stability of MoS_2 membrane in aqueous environment and size-dependent selectivity of ions have been reported.[35] However, contradictory observations from other studies, including low water flux in osmotic processes[36] and potential application of MoS_2-layered structure as non-permeable film for corrosion control,[38,39] suggest that it is important to comprehensively characterize the nanostructure of MoS_2 membranes and fundamentally understand their separation performance. In addition, so far there has been a lack of mechanistic insights into the swelling behavior of MoS_2 membranes in aqueous environment and the ionic/molecular transport through MoS_2 nanochannels.

In the present study, we systematically elucidated the mechanisms for the nanostructural stability and water filtration capability of layer-stacked MoS_2 membranes in aqueous environment. To achieve this goal, the stability (i.e., anti-swelling) of MoS_2 membranes in water was investigated by measuring the changes in the membrane mass and interlayer spacing as well as by analyzing the interaction forces between MoS_2 nanosheets. In addition, both experimental characterization and molecular dynamics (MD) simulation were performed to thoroughly study the water transport inside MoS_2 nanochannels. The separation capability of MoS_2 membranes was evaluated using representative ionic species and organic dyes.

Preparation and Properties of MoS_2 Nanosheets. MoS_2 nanosheets were prepared by an established chemical exfoliation method, that is, organolithium intercalation followed by forced hydration.[40,41] As schematically illustrated in Figure 1a-c, the lithium intercalation weakens the original attractions between neighboring MoS_2 layers within a bulk, and further expands the interlayer spacing by generating hydrogen gas once lithium reacts with water. A dispersion of chemically exfoliated MoS_2 (ce-MoS_2) was thus generated with the assistance of sonication and used to make layer-stacked membranes *via* pressure-assisted filtration (Figure 1d). The obtained MoS_2 nanosheets were mostly in monolayer form, as shown in the atomic force microscopy (AFM) image (Figure 1e), and the hydrodynamic size was determined by dynamic light scattering as 304 nm (Supporting Information Figure S1a). X-ray photoelectron spectroscopy (XPS) analyses in

Figure 1f and Supporting Information Figure S1b reveal that the ce-MoS_2 was a mixture of metallic 1T phase (dominant component) and semiconducting 2H phase, unlike the pure 2H phase in the bulk counterpart. Furthermore, UV-vis spectra (Supporting Information Figure S1c) also confirm the predominance of the 1T phase in the as-prepared MoS_2. In addition to phase transformation during the intercalation process, electrons are believed to transfer from the organolithium reagent to MoS_2,[42] leading to a high negative charge density with a zeta potential of -55 mV in neutral pH condition (Supporting Information Figure S1d) and thus good water dispersibility.

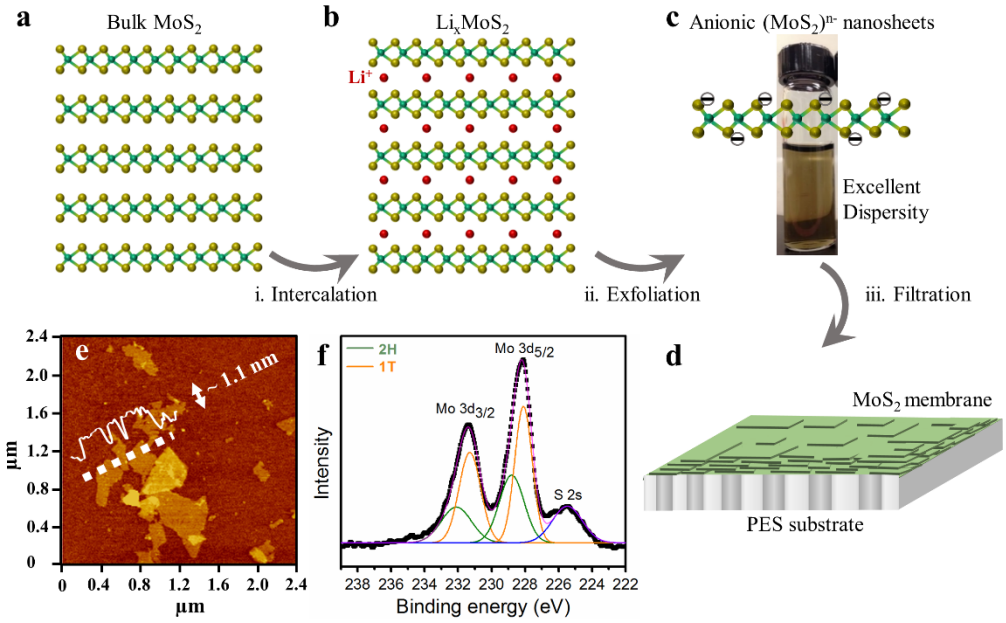

Figure 1. Schematic illustration of the MoS_2 membrane preparation process and characterization of chemically-exfoliated MoS_2 nanosheets. The process includes three steps: Li intercalation of bulk MoS_2 (a) to obtain Li_xMoS_2 (b), followed by the exfoliation of Li_xMoS_2 into dispersed MoS_2 nanosheets (c), and lastly the deposition of restacked MoS_2 membrane on top of a polyethersulfone (PES) substrate by pressure-assisted filtration (d). (e) The obtained MoS_2 nanosheets were primarily monolayers with a thickness of ~ 1.1 nm, as measured by AFM. (f) XPS spectra of exfoliated MoS_2 nanosheets indicate that the phase conversion resulted in the metallic 1T phase as a dominant phase.

Preparation of MoS_2 Membrane. The layer-stacked MoS_2 membrane was prepared with the as-synthesized ce-MoS_2 nanosheets by pressure (0.7 bar or 10 psi)-assisted filtration onto a polyethersulfone (PES) ultrafiltration substrate, which has a nominal pore size of around 30 nm. As shown in Supporting Information Figure S2a, it typically took ~30 min to filter 10 ml of MoS_2 solution (0.5 mg/mL) to make a membrane with a thickness of ~ 1 µm, while it took almost a day

to make a GO membrane with similar thickness. The faster filtration process indicates that a MoS_2 membrane most likely has much higher water permeability than a comparable GO membrane. Furthermore, we discovered that the prepared MoS_2 membrane must be kept in wet/hydrated condition in order to maintain its filtration capability, as the oven-dried (at 60 °C for 2 h) MoS_2 membrane almost entirely lost its water permeability. As shown in Supporting Information Figure S2b, the dry MoS_2 membrane was impermeable to water for at least 6 h under a pressure up to 4.1 bar (60 psi). This observation is consistent with the results from a recent study that reported ultralow permeance of water and small ionic species through MoS_2 membranes even under a high osmotic pressure (1 M NaCl)[35] as well as from other studies that used MoS_2 membranes as anti-corrosion coatings.[38,39]

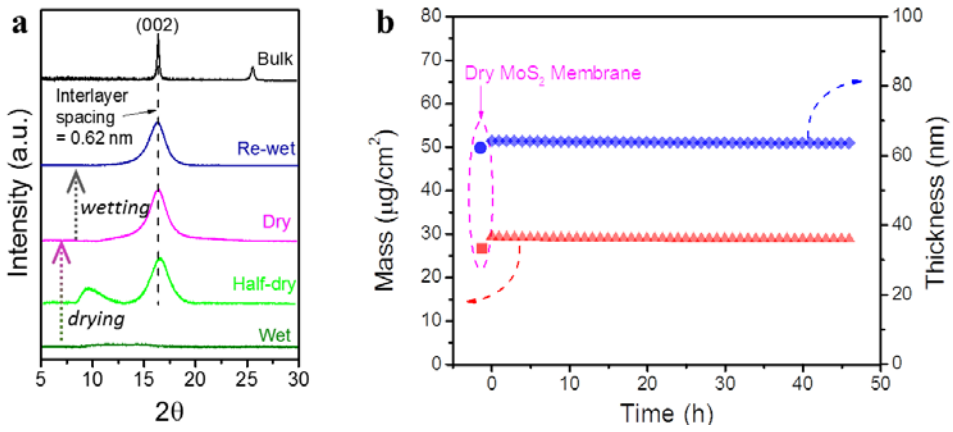

Figure 2. The irreversible restacking of completely dried MoS_2 nanosheets. (a) XRD patterns of MoS_2 membranes showed the evolution of characteristic peaks during a drying and re-wetting process, implying the dry MoS_2 membrane had an interlayer spacing of 0.62 nm similar to that of bulk MoS_2, and this interlayer spacing remained unchanged after the dry MoS_2 membrane was re-wetted for one day. (b) The mass and thickness of the dry MoS_2 membrane, as measured by QCM-D coupled with ellipsometry, remained unchanged during 2-day soaking in water.

Consistently, the X-ray diffraction (XRD) characterization (Figure 2a) shows that the intensive peak (002) of the dry MoS_2 membrane was located at 2θ of 16.4°, corresponding to an interlayer spacing of merely 0.62 nm (or 0.3-nm free spacing), which is essentially the same as that of bulk MoS_2 and too narrow for water molecules to pass through.[31] In contrast, the XRD signal of the hydrated MoS_2 membrane was significantly weakened not only due to the X-ray absorption by the water molecules within MoS_2 nanochannels but also due to the less ordered long-range structure as a result of water layer fluctuation.[43,44] Note that a peak started to appear halfway through the drying process, indicating that the interlayer spacing was reduced and became

measurable as the MoS_2 membrane was gradually dried. To confirm that the enlarged spacing between hydrated MoS_2 nanosheets was caused by the intercalation of water molecules, the wet MoS_2 membrane was treated by freeze-drying with liquid nitrogen, creating an apparently more porous structure (Supporting Information Figure S3) due to the crystallization and evaporation of water molecules during the freeze-drying process. In addition, the restacking of MoS_2 nanosheets caused by drying was irreversible, as evidenced by the unchanged XRD peak position after the dry MoS_2 membrane was soaked in water for one day (referred to as the re-wetted sample in Figure 2a). Another evidence is that the mass and thickness of the dry MoS_2 membrane in water remained unchanged for at least 2 days (Figure 2b), as measured by QCM-D coupled with ellipsometry.

Structure and Stability of MoS_2 Membranes without Crosslinking. The cross-sectional SEM images of the dry MoS_2 membrane exhibit a typical layered structure (Figure 3a) with a long-range uniform thickness (Supporting Information Figure S4a). The energy dispersive X-ray spectroscopy (EDS) analysis (Supporting Information Figure S4b) showed a uniform distribution of molybdenum and sulfur with an approximate ratio of 1:2, while such elements were not obviously observed in the PES substrate after the removal of the MoS_2 film, indicating the absence of MoS_2 penetration into the PES substrate.

The stability of fully hydrated MoS_2 membranes in aqueous solution was compared with that of GO membranes. GO and MoS_2 membranes with similar thickness were freshly prepared under the same filtration conditions (Figure 3b), and the wet and fully hydrated membranes thus synthesized were subsequently soaked in water with mild agitation at 200 rpm using a shaking table. It was observed that the GO membrane quickly disintegrated into pieces after 1 min (Figure 3c), small particles after 30 min (Figure 3d), and very fine powders after 1 h clearly evidencing the re-dispersion of GO nanosheets since the solution turned brownish (Figure 3e). In contrast, the MoS_2 membrane remained intact throughout a similar soaking and agitation process, although the GO and MoS_2 nanosheets have similar charge properties and hydrophilicity (Supporting Information Figures S1d and S5).[45] The supernatants from the soaking solutions were then measured by UV-vis absorption. As shown in Figure 3f, the presence of a characteristic peak of GO at ~ 250 nm confirmed the existence of re-dispersed GO nanosheets, whereas the absence of any characteristic peak of MoS_2 verified that no MoS_2 nanosheets were released from the membrane. The above comparison implies that the MoS_2 membrane, even in its fully hydrated

state with an enlarged interlayer spacing, still possesses excellent stability in water without the assistance of any crosslinker between individual layers.

Non-swelling MoS_2 vs. Swelling GO. Because the accuracy of XRD in measuring a relatively large interlayer spacing is lowered by weakened signals, ellipsometry was used instead to obtain the interlayer spacing of a MoS_2 membrane. To do so, we measured h_d and h_w, the thicknesses of oven-dried and wet MoS_2 membranes, respectively. Taken 0.62 nm as the interlayer spacing of an oven-dried MoS_2 membrane (Figure 2a), the interlayer spacing d_w of a wet MoS_2 membrane can be calculated as $0.62 \cdot h_w/h_d$. Figure 3g shows that the interlayer spacing of a wet MoS_2 membrane did not change over three days of soaking, indicating the MoS_2 membrane did not further swell over time after it was hydrated at the beginning. Based on three repeated measurements, we calculated the interlayer spacing of a wet MoS_2 membrane to be 1.2 ± 0.1 nm. This relatively constant interlayer spacing would lead to stable separation performance of MoS_2 membranes in aqueous environment. Deducting the thickness (0.3 nm) of a MoS_2 layer[31] from the calculated interlayer spacing, we estimate the free spacing of a wet MoS_2 nanochannel to be 0.9 ± 0.1 nm, which is capable of separating multivalent ions and many organic molecules from water. In comparison, the interlayer spacing of a GO membrane in a same soaking experiment gradually increased from 0.8 to 5.2 nm (Figure 3g), indicating the GO membrane swelled significantly in water.

The above membrane behavior can be explained by analyzing the interaction forces between nanosheets. Based on the extended DLVO theory,[46] the equilibrium interlayer spacing is most likely controlled by the balance among the electrostatic repulsion, hydration, and van der Waals (vdW) attraction forces. Because MoS_2 and GO nanosheets have similar hydrophilicity and carry almost the same amount of negative charge, their electrostatic repulsion and hydration forces can both be estimated using Supporting Information Eqs. S1-6. As shown in Figure 3h, the electrostatic repulsion is almost negligible and the hydration force is the predominant repulsive force with less than 2-nm free spacing in the present study.

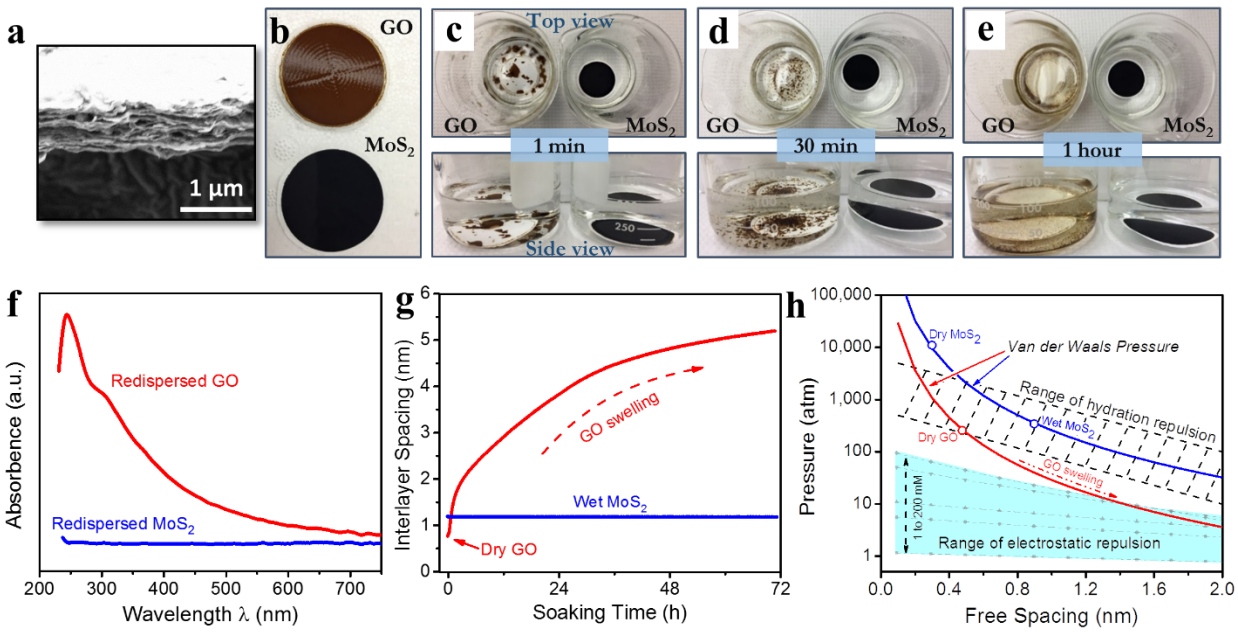

Figure 3. Comparison of the stability of wet MoS_2 and GO membranes. (a) Cross-sectional SEM image of the laminar structure of a dry MoS_2 membrane. As the membrane-containing bulk was mildly stirred at 200 rpm on a shaking table, the freshly prepared ~1-μm-thick GO membrane (b) readily disintegrated in water after 1 min (c), 30 min (d), and 1 h (e), whereas the wet MoS_2 membrane having similar thickness remained intact. (f) At 1 h, the GO membrane-containing solution showed the characteristic absorption peak of GO nanosheets, while no MoS_2 nanosheets were found to be released into the corresponding solution. (g) The interlayer spacing of wet MoS_2 and GO membranes (measured by ellipsometry) as a function of soaking time. (h) Comparison of van der Waals, electrostatic repulsion, and hydration forces, as a function of free spacing, in the MoS_2 and GO membranes. The electrostatic repulsion is estimated considering nanosheets with a surface potential of -55 mV in 1 to 200 mM NaCl solutions.

The vdW attraction between two nanosheets is estimated using a simplified parallel surface model[47]:

$$P_{vdW} = \frac{A_{131}}{6\pi D^3} \tag{1}$$

where D is the free spacing (i.e., interlayer spacing excluding a nanosheet thickness) between two nanosheets, and A_{131} is the Hamaker constant of two identical phase 1 interacting across medium 3, which is defined by

$$A_{131} = \frac{3kT}{4}\left(\frac{\varepsilon_1-\varepsilon_3}{\varepsilon_1+\varepsilon_3}\right)^2 + \frac{3h\omega}{16\sqrt{2}}\frac{(n_1^2-n_3^2)^2}{(n_1^2+n_3^2)^{3/2}} \tag{2}$$

where k is the Boltzmann constant, $1.38\times10^{-23}J/K$; T is the absolute temperature, $293K$; ε_1 is the dielectric constant of MoS_2 (3.7) or GO (3.0);[48,49] ε_3 is the static dielectric constant of water, 80.1; h is the Planck's constant, $6.63\times10^{-34}J\cdot s$; ω is the absorption frequency, $4.73\times10^{14}s^{-1}$; n_1 is the refractive index of MoS_2 (2.7) or GO (1.6); and n_3 is the refractive index of

water, 1.33 in visible light regime as determined by ellipsometry. Therefore, the Hamaker constants of MoS_2 and GO nanosheets in water are calculated to be $48.9 \times 10^{-21}\,J$ and $5.47 \times 10^{-21}\,J$, respectively.

As exhibited in Figure 3h, the MoS_2 nanochannel has a much stronger vdW attraction force than the GO nanochannel. In addition, the vdW attraction between neighboring GO nanosheets falls below the estimated range of hydration force (denoted as the dash-hatched area in Figure 3h), implying that the hydration force can overcome the relatively weak vdW attraction to initiate the GO membrane swelling. As a result, the long-range electrostatic force starts to play a role and eventually becomes the dominating force in the fully swelled GO membrane. In contrast, the strong vdW force of the MoS_2 membrane provides sufficient attraction to prevent its interlayer spacing from increasing. In particular, the vdW force associated with the dry MoS_2 membrane is so large that its interlayer spacing of 0.62 nm remains unchanged even after being soaked in water for two days (Figure 2), thereby explaining the irreversible restacking of MoS_2 nanosheets by drying. Besides, as the free spacing between the nanosheets of a wet MoS_2 membrane increases, the vdW force decreases significantly. At a free spacing of ~0.9 nm, the vdW force becomes equal in magnitude to the average hydration force (Figure 3h), reaching an equilibrium (stable) state of the MoS_2 nanochannel.

Water Flux of MoS_2 Membranes. Fast compaction of freshly prepared MoS_2 membranes under transverse pressure was implied from the water permeability test. As shown in Supporting Information Figure S6a, a ~500 nm-thick MoS_2 membrane initially exhibited a constant water flux of 140 LMH when tested at 0.7 bar (10 psi), or 200 LMH/bar, which is in the same range as the reported ~ 245 LMH/bar for a micrometer-thick membrane.[26] However, upon the increasing of pressure with a increment of 0.7 bar, the water flux promptly increased (due to higher driving force) but then quickly decreased and reached a much lower, nearly steady-state level (due to membrane compaction). After a pressure of 4.1 bar (60 psi) was applied, the pressure was gradually decreased by 0.7 bar at a time. At each lowered pressure level, the water flux dropped proportionally and became steady immediately. At the end of the test, the pressure was removed from the membrane, which was tested again on the next day using an identical procedure. It is observed in Supporting Information Figure S6b that the day-2 water flux was immediately steady at each pressure level, irrespective of an increasing or decreasing pressure phase, indicating that the compaction of the

MoS_2 membrane during day 1 was irreversible.

Such behavior of the MoS_2 membrane under a varying pressure is completely different from that of a GO membrane tested using a very similar procedure with a pressure varying from 0.7 to 4.8 bar.[23] In contrast to the steady flux vs. applied pressure relationships of the MoS_2 membrane over the two-day test, as summarized in Supporting Information Figure S6c, almost indistinguishable nonlinear flux-pressure relationships of the GO membrane were reported,[23] indicating elastic (and hence reversible) deformation of the GO membrane. Considering the aqueous stability of the MoS_2 membrane, we hypothesize that the applied pressure, which was generally higher than that used in membrane preparation (0.7 bar), further organized the layered structure of the MoS_2 membrane by reducing/eliminating the larger pores and/or channels caused by random restacking, as schematically illustrated in Supporting Information Figure S7. To confirm such a compressed structure, direct morphological and structural characterizations are necessary and planned as future work. The resulting MoS_2 membrane with mostly rigid nanochannels contributed to the linear flux-pressure relationship (Supporting Information Figure S6C). Therefore, it is beneficial to apply a relatively high pressure during MoS_2 membrane preparation in order to form a neatly stacked structure with minimum voids or looseness, leading to both consistent and improved selectivity. In the following discussion, MoS_2 membranes were first compacted with a high pressure of 4.1 bar to eliminate any loose structure prior to permeability and separation tests.

The water flux data of MoS_2 membranes obtained from the present study are compared in Figure 4a with those of GO membranes available in the literature, with detailed information on their properties and performance provided in Supporting Information Table S1. Depending on membrane thickness, the water flux of MoS_2 membranes varies between 30 and 250 LMH/bar, which is in general much higher (2-10 times) than that of GO membranes prepared by vacuum filtration (blue symbols) or layer-by-layer/LbL assembly (green symbols), while inserting large spacers between GO layers could increase the water flux of GO membranes (red symbols with dots) at the cost of sacrificing their capability in rejecting small ionic/organic species.

It is important to note that the MoS_2 membranes in fully dried vs hydrated states exhibit dramatically different water transport behaviors, which can be explained by considering the interlayer spacing of MoS_2 membranes in different hydration states. When a MoS_2 membrane is fully hydrated, its interlayer spacing is maintained at 1.2 nm to allow fast water transport through

the MoS_2 nanochannel. However, once a MoS_2 membrane is dried during fabrication or storage, its interlayer spacing decreases to 0.62 nm. As discussed earlier, the corresponding restacking of MoS_2 nanosheets is an irreversible process, that is, the dried MoS_2 membrane is unable to be hydrated/re-wetted in water and thus it is nearly impermeable to water.

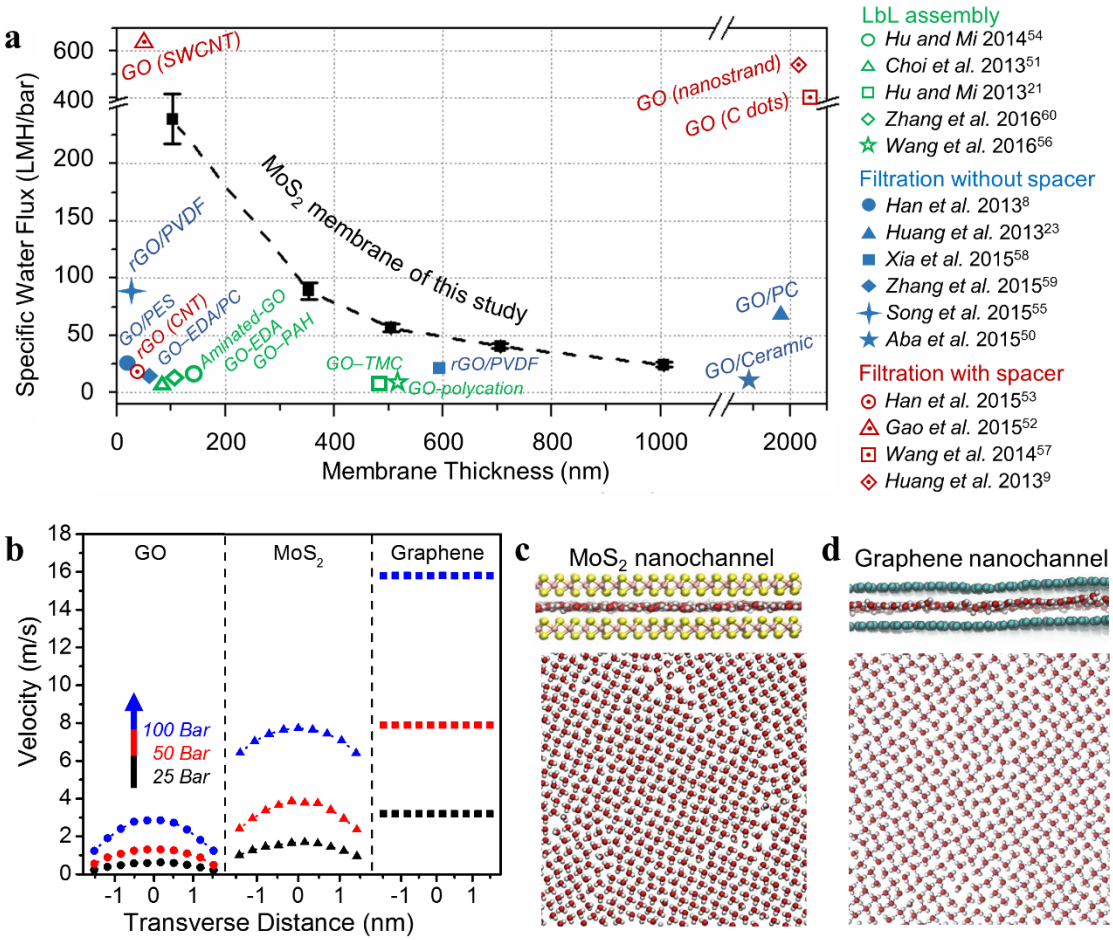

Figure 4. Understanding the fast water filtration through MoS_2 membranes. (a) Experimental measurements revealing the thickness-dependent water flux of MoS_2 membranes, in comparison with data of GO-based membranes (measured in a pressure-driven system) from literature.[8,9,21,23,50-60] (b) The velocity profiles of GO, MoS_2 and pristine graphene nanochannels by MD simulations. Side and top views of single-layer water molecules in the MoS_2 nanochannel (c) and graphene nanochannel (d), each showing the alignment of water molecules in a rhombus-shaped network.

To fundamentally understand the fast water flux of MoS_2 membranes, we used MD simulation to investigate water transport in the MoS_2 nanochannel under different pressures (25, 50, and 100 bars, respectively) and compared it with that in GO and graphene nanochannels, respectively. Note that both MoS_2 and graphene have well-defined single-layer crystalline structures, while GO has a chemically irregular morphology due to the uncertain distribution of

different functional groups. A detailed description of the modeling of all three materials can be found in the Supporting Information. As shown in Figure 4b, the velocity profile in the MoS_2 nanochannel at each pressure level takes a parabolic shape. A slip velocity can be obtained by averaging the velocity values of all water molecules within the first water layer, which is ~ 0.32 nm away from the nanochannel wall. The slip velocity in the MoS_2 nanochannel increases with increasing pressure (i.e., 1.2, 3.3, and 7.2 m/s under 25, 50, and 100 bars, respectively), and is about 3-4 times the slip velocity in the GO nanochannel (i.e., 0.34, 0.9, and 1.9 m/s under 25, 50, and 100 bars, respectively). Note that a fast slip velocity in general amounts to a high water flux in the nanochannel, consistent with the observation in Figure 4a that the water flux of MoS_2 membranes is higher than that of GO membranes. Such a flux difference is most likely attributed to the lower hydraulic resistance of the smoother, more rigid MoS_2 nanochannel as well as the higher hydraulic resistance of the GO nanochannel due to the extrusion of oxygenated functional groups from the GO basal plane.

Particularly, our MD simulation revealed that the single-layer water molecules confined in both MoS_2 and graphene nanochannels exhibit a well-aligned, rhombus-shaped network (Figure 4c-d), which has been confirmed experimentally in graphene nanocapillaries.[61] Such water alignment is attributed to the lack of hydrogen bonding at the water-surface interface and has been associated with the fast water permeation through the nanocapillaries in carbon nanotube and graphene membranes.[61,62] The well-aligned water structure in our MoS_2 nanochannels is also consistent with the finding from a recent MD study, which revealed that such an aligned pattern is mainly caused by the H-bonds within the water network.[63] As shown in Figure 4b, under the same pressure, the velocity in the pristine graphene nanochannel is the highest and has a horizontal profile, which differs remarkably from the parabolic shape for GO and MoS_2 nanochannels. This is because significant boundary slip exists in the pristine graphene nanochannel due to the diminishing friction at the liquid-solid interface.[17] For the graphene nanochannel, the water velocity is uniform over the cross-section of the nanochannel and thus equal to the slip velocity, which are 3.2, 7.9 and 15.8 m/s under 25, 50, and 100 bars, respectively.

MD simulation also enabled us to theoretically verify the water flux data obtained experimentally. Considering the computational cost, we built a simplified multilayer MoS_2 model (Section 4 of Supporting Information) instead of a model with a thickness of hundreds of nanometer. Simulation results in Figure S9 indicate that the overall water flux of a MoS_2 membrane

may be approximately inversely proportional to the membrane thickness. Thus, for a 500-nm-thick MoS_2 membrane (the one used in the separation tests as discussed below), the water flux should be approximately 50 LMH/bar, matching the experimental result very well (Figure 4a).

Note that, in addition to interlayer spacing and water/membrane interface interactions, other specific microstructural features of the restacked nanosheets may also influence the water flux of MoS_2 and GO membranes. For example, smaller lateral dimensions of nanosheets and the presence of pores/defects on nanosheets are expected to shorten the pathway for water molecules and thus increase water flux. However, in order to understand such effects on the flux behaviors of MoS_2 and GO membranes, the membrane microstructure should be experimentally tuned and characterized, followed by systematic investigation of the corresponding membrane performance.

Separation Performance of MoS_2 Membranes. The separation capability of layer-stacked MoS_2 membranes was evaluated using representative ionic species and organic dyes. During the rejection experiments with a 500-nm-thick MoS_2 membrane, constant water permeability was observed (Figure 5a) as the test solutions were switched between deionized water and NaCl solutions (20, 200 mM), confirming the rigidity and stability of MoS_2 nanochannels under different ionic strength conditions. This observation is also consistent with the analysis in Figure 3h that the vdW force is dominant in the MoS_2 nanochannel and thus the change in the electrostatic repulsion due to the change in ionic strength cannot vary the net interactions or interlayer spacing. Furthermore, the effect of ionic strength on the interlayer spacing was studied using ellipsometry measurements, which confirmed that the interlayer spacing of MoS_2 nanochannels stays almost the same in different ionic strength conditions (Supporting Information Figure S10). In comparison, the GO nanochannel is relatively elastic and, as a result, it becomes narrower and thus water permeation decreases in higher ionic strength solutions due to the compression of electric double layers.[23]

Rejection experiments were carried out using sodium-based ionic species with mono-, di-, or tri-valent anions (chloride, acetate, sulfate and citrate). As shown in Figure 5b, the 500-nm-thick MoS_2 membrane exhibited high rejection (~ 55-70%) of all ionic species when the ionic strength was low (< 2 mM). However, the rejection of ionic species decreased noticeably with the increasing ionic strength of the solution, most likely due to the compression of double layers and the decrease of surface zeta potential (Supporting Information Figure S11). In addition, the MoS_2

membrane showed better rejection of di- and multivalent anions (sulfate and citrate), again demonstrating that the rejection mechanism is dominated by electrostatic repulsion between the negatively charged MoS_2 membrane and anions.

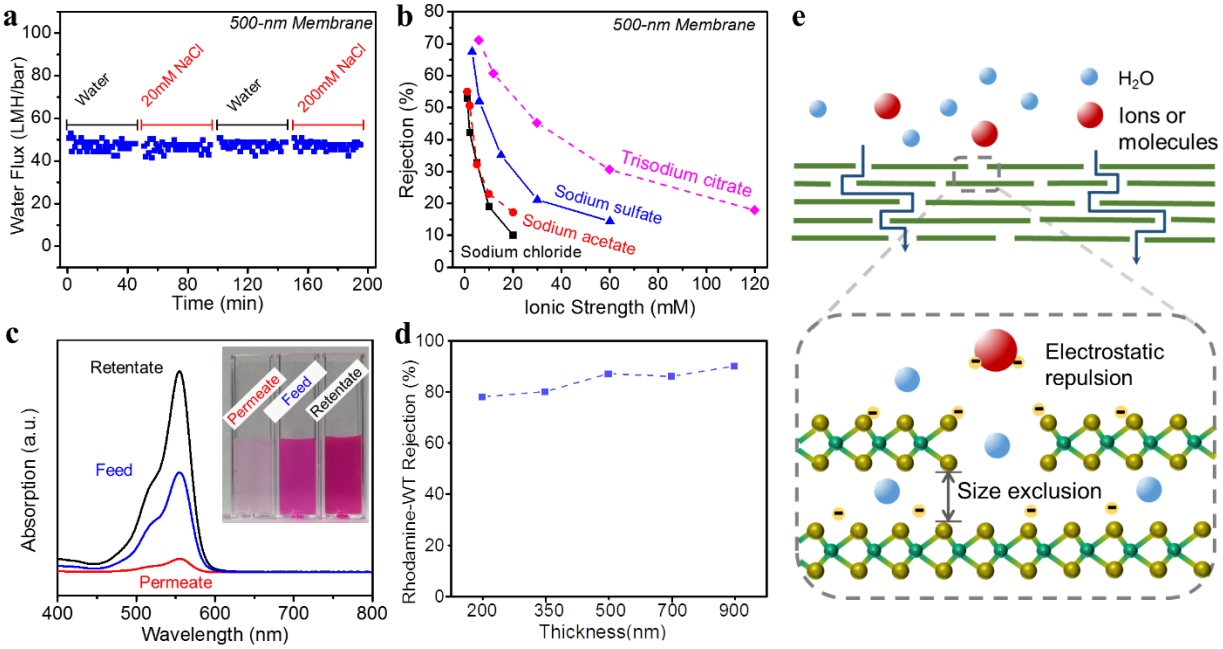

Figure 5. The performance and mechanism of MoS_2 membranes in rejection of ionic species and organic dyes. (a) The steady water permeance of a 500-nm-thick MoS_2 membrane in filtering water and salt solutions (20, 200 mM NaCl). (b) Effects of solute charge and ionic strength of solutions on the rejection of ionic species. (c) The concentrations of organic dye (Rhodamine-WT) in permeate, feed, and retentate, as evidenced by the absorption spectra. The inset optical image shows the nearly colorless permeate and concentrated retentate, as compared to the feed solution. (d) Dependency of organic dye rejection on MoS_2 membrane thickness. (e) The proposed mechanisms of MoS_2 membranes include both size exclusion and electrostatic repulsion.

MoS_2 membranes were also tested for the removal of organic dyes using model compounds, including negatively charged Rhodamine-WT and positively charged Methylene blue. The dye concentrations in the permeate and retentate solutions were monitored by UV-vis analysis. As shown in Figure 5c, the retentate solution was concentrated with the absorbance twice as much as that of the feed solution after the same volume of permeate solution was collected, implying insignificant physical adsorption of negatively charged Rhodamine-WT. Typically, the removal of Rhodamine-WT by the 500-nm-thick MoS_2 membrane was as high as 90%. The increase in MoS_2 membrane thickness (from 200 to 900 nm) did not improve the rejection significantly (Figure 5d), further confirming the negligible role of adsorption in the separation of Rhodamine-WT molecules. The rejection of Rhodamine-WT by our MoS_2 membrane is similar to the rejection of Evans blue

obtained in a previous study,[26] although Rhodamine-WT has a smaller molecular weight (487 vs. 961)[21] and a smaller Stokes radius (1.1-1.2 nm, as calculated using Supporting Information Equation S8, vs. 2.8 nm)[64,65]. The capability of removing smaller molecules was possibly due to the compaction of loose MoS_2 structure by high pressure after membrane preparation in our study.

The rejection of positively charged Methylene blue by the 500-nm-thick MoS_2 membrane was initially 100% but decreased to a stable level of ~ 40 % (Supporting Information Figure S12). The initial high rejection was due to physical adsorption on the anionic MoS_2 nanosheets. At the end of the test, Methylene blue was also concentrated in the retentate, indicating a size exclusion mechanism after the saturation of membrane adsorption capacity. We believe that the overall separation mechanisms for organic dye separation by a MoS_2 membrane include both size exclusion and electrostatic repulsion (Figure 5e).

In conclusion, we have shown that, unlike layer-stacked GO membranes that tend to disintegrate in aqueous environment, layer-stacked MoS_2 membranes possess an excellent anti-swelling property with a stable 1.2-nm interlayer spacing (or 0.9-nm free spacing) for hydrated nanochannels. We have attributed this aqueous stability to the equilibrium between the short-range attractive van der Waals and repulsive hydration forces. As a result, crosslinking of restacked MoS_2 nanosheets is not needed, an advantage that simplifies the synthesis procedure, reduces the production cost, and potentially improves the membrane performance due to the absence of crosslinkers that impede water flow within the membrane. We have also demonstrated that the water flux of MoS_2 membranes is much higher than that of GO membranes having similar thickness, and we have attributed this high water permeability to the low hydraulic resistance of the smooth, rigid MoS_2 nanochannels. Besides, we have fundamentally elucidated the remarkably different, water-impermeable behavior of the dry MoS_2 nanochannel, which has a 0.62-nm interlayer spacing (or 0.3-nm free spacing), caused by the irreversible nanosheet restacking during a drying process. It is emphasized that, despite the promise of MoS_2 membranes as demonstrated in the present study, much needs to be done to gain a complete knowledge of their nanostructure and various properties toward enhanced water filtration and separation performance. Finally, it is worth noting that the methods that integrate experiments and simulation for the present MoS_2 study should prove useful for the performance evaluation and mechanistic understanding of other 2D nanomaterials for potential membrane-based applications.

Preparation of 2D Nanomaterials and Layer-stacked Membranes. A dispersion of GO nanosheets was prepared from graphite using the modified Hummers' method.[66,67] MoS_2 nanosheets were prepared by a chemical exfoliation method.[40] Typically, in a nitrogen-filled glove box, 300 mg of MoS_2 powder (Sigma-Aldrich, Saint Louis, MO) was dispersed in 3 mL of 1.6 M n-butyllithium hexane solution (Sigma-Aldrich, Saint Louis, MO) under moderate stirring for lithium intercalation. After reaction for 2 days, the resulting lithium-intercalated product was rinsed twice with hexane to remove the excess organolithium reagent and organic by-products, and then immediately exfoliated into nanosheets by reaction with deionized water in an ultrasonic bath for 1 h. Un-exfoliated MoS_2 was removed by centrifugation at 500 rpm for 10 min. The supernatant was subjected to dialysis (3.5K MWCO Tubing, Thermo Scientific, Saint Louis, MO) in water to remove the inorganic by-products (*e.g.*, LiOH). Dispersions of chemically exfoliated MoS_2 samples were stored in a glove box. The layer-stacked GO membrane and MoS_2 membrane were each assembled by pressure-assisted filtration in a stirred cell (50 mL, Amicon, Billerica, MA) on a porous PES substrate (Sterlitech, Kent, WA) with a nominal pore size of 30 nm. The membrane thickness was controlled by the volume and concentration of the dispersion. In a typical experiment, 5 mL of 0.5 mg/mL MoS_2 solution led to a membrane thickness of about 500 nm, and a GO membrane of the same thickness was prepared with 10 mL of 0.1 mg/mL GO dispersion.

Integrated QCM-D/Ellipsometry Measurement. The swelling of MoS_2 and GO membranes in aqueous environment was each characterized by using an integrated system of QCM-D and ellipsometry.[68] As illustrated in Supporting Information Figure S13, this system was set up by mounting an ellipsometry-specified QCM-D module (E-1, Biolin, Sweden) on the sample stage of a multi-wavelength ellipsometer (FS-1Multi-wavelength, Film Sense, Lincoln, NE). The QCM-D module has a glass lens on each side, through which the incident light from the light source shines on the sample and reflects back to the detector. As the first step, a bare gold-sensor was characterized in a dry state and then in aqueous environment by the integrated system to collect the oscillation frequency and energy dissipation (for QCM-D analysis) as well as the complex refractive index (for ellipsometry analysis) of the gold sensor.

Preparation of the tested MoS_2 and GO thin films was each based on a transplanting method, which was elaborated in our previous study[68] and is briefly described here. The thin film was assembled on a PES support by filtration, and subsequently a clean gold-sensor was attached

onto the surface of the thin film with its topside facing the thin film. The thin film was then transplanted to the gold sensor after peeling the sensor off from the polymer support. Changes in the mass and thickness of the thin film in aqueous environment were simultaneously monitored by the integrated system. The dynamic mass change was model-fitted using the Voigt model[69] and the thickness change was fitted by a three-layer (Au-thin film-water) optical model.

Membrane Characterization. The top-view and cross-sectional images as well as the elemental analyses of a layer-stacked membrane were recorded and analyzed by a field emission SEM (Zeiss Gemini Ultra-55, Jena, Germany). Powder XRD was performed by using graphite-monochromated Co Ka radiation (λ = 0.179 nm) on a D8 Discover GADDS system (Bruker, Madison, WI). XPS analysis of samples was carried out using PHI 5400 XPS spectrometer (Perkin Elmer, Waltham, MA). The UV-vis absorbance spectra were collected from Genesys 10S UV-Vis (Thermo Scientific, Fremont, CA). Zeta potential measurements were conducted on a Zetasizer Nano-ZSP analyzer (Malvern, Westborough, MA).

Membrane Flux and Rejection Tests. Water flux and rejection performance were tested in a cross-flow configuration for dry MoS_2 membranes and in a stirred cell (50 mL, Amicon), where the tested membranes were prepared, for wet MoS_2 membranes at a stirring rate of 500 rpm. The hydraulic pressure was varied to study its effects on the water permeability of MoS_2 membranes. To test the permeance and ejection of various solutes, the MoS_2 membrane was first stabilized under a high compressive pressure of ~ 4.1 bar (60 psi) to achieve steady permeance. The concentrations of organic dyes in feed, permeate, and retentate solutions were measured by using UV–vis spectrophotometer. The concentration of an ionic aqueous solution was calculated according to its ionic conductivity. The rejection R of markers was calculated as $R = \left(1 - C_p/C_R\right) \cdot 100\%$, where C_p and C_R are the concentrations of markers in the permeate and retentate solutions, respectively.

MD Simulations. MD simulations were performed using GROMACS,[70,71] and the simulation results were processed and visualized by VMD.[72] The OPLS force fields,[73] which are well optimized for simulating fluid problems, were used to model the MoS_2 membrane as well as ions

and water molecules. The SPC/E model[74] was employed to describe water molecules. The simulation was carried out with a time step of 2 fs. Each system was simulated for 5 ns followed by an equilibration under the NVT ensemble (constant number of atoms, fixed volume, and constant temperature of 298 K). The Nose-Hoover thermostat[75] was used to maintain the temperature at 298 K, and then the non-equilibrium MD simulation was performed[76] by adding constant acceleration in one direction to each atom. The PME (Particle-mesh Ewald) method was employed to accurately account for the long-range electrostatic interactions of the charges or ions and their periodic images. The cut-off of the Lennard-Jones (LJ) interactions was set at 1.2 nm in all three directions. Additional information is provided in Supporting Information.

Associated Content

Supporting Information

Additional figures, detailed calculations of electrostatic repulsion and hydration force between nanosheets, detailed information on MD simulation of MoS_2 membranes, and a table summarizing the separation performance of GO-based membranes (PDF).

Acknowledgements

The material is based upon work supported by the U.S. National Science Foundation under award no. CBET-1565452 and CBET-1706059. Work at the Molecular Foundry was supported by the Office of Science, Office of Basic Energy Sciences, of the U.S. Department of Energy under contract no. DE-AC02-05CH11231. The opinions expressed herein, however, are those of the authors and do not necessarily reflect those of the sponsors.

References

(1) Joshi, R.; Carbone, P.; Wang, F.-C.; Kravets, V. G.; Su, Y.; Grigorieva, I. V.; Wu, H.; Geim, A. K.; Nair, R. R. *Science* **2014,** 343, 752-754.
(2) Lei, W.; Mochalin, V. N.; Liu, D.; Qin, S.; Gogotsi, Y.; Chen, Y. *Nat. Commun.* **2015,** 6, 8849
(3) Ding, L.; Wei, Y.; Wang, Y.; Chen, H.; Caro, J.; Wang, H. *Angew. Chem. Int. Ed.* **2017,** 56, 1825–1829.
(4) Varoon, K.; Zhang, X.; Elyassi, B.; Brewer, D. D.; Gettel, M.; Kumar, S.; Lee, J. A.; Maheshwari, S.; Mittal, A.; Sung, C.-Y. *Science* **2011,** 334, 72-75.
(5) Sun, L.; Ying, Y.; Huang, H.; Song, Z.; Mao, Y.; Xu, Z.; Peng, X. *ACS Nano* **2014,** 8, 6304-6311.
(6) Mi, B. *Science* **2014,** 343, 740–742.
(7) Mishra, A. K.; Ramaprabhu, S. *Desalination* **2011,** 282, 39-45.
(8) Han, Y.; Xu, Z.; Gao, C. *Adv. Funct. Mater.* **2013,** 23, 3693-3700.
(9) Huang, H.; Song, Z.; Wei, N.; Shi, L.; Mao, Y.; Ying, Y.; Sun, L.; Xu, Z.; Peng, X. *Nat. Commun.* **2013,** 4, 2979.
(10) Zheng, S.; Mi, B. *Environ. Sci.: Water Res. Technol.* **2016,** 2, 717-725.
(11) Oh, Y.; Armstrong, D. L.; Finnerty, C.; Zheng, S.; Hu, M.; Torrents, A.; Mi, B. *J. Membr. Sci.* **2017,** 541, 235-243.
(12) Huang, K.; Liu, G.; Lou, Y.; Dong, Z.; Shen, J.; Jin, W. *Angew. Chem. Int. Ed.* **2014,** 53, 6929-6932.
(13) Liu, R.; Arabale, G.; Kim, J.; Sun, K.; Lee, Y.; Ryu, C.; Lee, C. *Carbon* **2014,** 77, 933-938.
(14) Hu, M.; Zheng, S.; Mi, B. *Environ. Sci. Technol.* **2016,** 50, 685-693.
(15) Perreault, F.; Tousley, M. E.; Elimelech, M. *Environ. Sci. Technol. Lett.* **2013,** 1, 71-76.
(16) Lee, J.; Chae, H.-R.; Won, Y. J.; Lee, K.; Lee, C.-H.; Lee, H. H.; Kim, I.-C.; Lee, J.-m. *J. Membr. Sci.* **2013,** 448, 223-230.
(17) Nair, R.; Wu, H.; Jayaram, P.; Grigorieva, I.; Geim, A. *Science* **2012,** 335, 442-444.
(18) Su, Y.; Kravets, V.; Wong, S.; Waters, J.; Geim, A.; Nair, R. *Nat. Commun.* **2014,** 5, 4843
(19) Talyzin, A. V.; Hausmaninger, T.; You, S.; Szabó, T. *Nanoscale* **2014,** 6, 272-281.
(20) Yeh, C.-N.; Raidongia, K.; Shao, J.; Yang, Q.-H.; Huang, J. *Nat. Chem.* **2015,** 7, 166-170.
(21) Hu, M.; Mi, B. *Environ. Sci. Technol.* **2013,** 47, 3715-3723.
(22) Liu, H.; Wang, H.; Zhang, X. *Adv. Mater.* **2015,** 27, 249-254.
(23) Huang, H.; Mao, Y.; Ying, Y.; Liu, Y.; Sun, L.; Peng, X. *Chem. Commun.* **2013,** 49, 5963-5965.
(24) Abraham, J.; Vasu, K. S.; Williams, C. D.; Gopinadhan, K.; Su, Y.; Cherian, C. T.; Dix, J.; Prestat, E.; Haigh, S. J.; Grigorieva, I. V. *Nat. Nanotechnol.* **2017,** 12, 546–550.
(25) Willcox, J. A.; Kim, H. J. *ACS Nano* **2017,** 11, 2187-2193.
(26) Sun, L.; Huang, H.; Peng, X. *Chem. Commun.* **2013,** 49, 10718-10720.
(27) Jiang, J.-W.; Qi, Z.; Park, H. S.; Rabczuk, T. *Nanotechnology* **2013,** 24, 435705.
(28) Chhowalla, M.; Shin, H. S.; Eda, G.; Li, L.-J.; Loh, K. P.; Zhang, H. *Nat. Chem.* **2013,** 5, 263-275.
(29) Chou, S. S.; Kaehr, B.; Kim, J.; Foley, B. M.; De, M.; Hopkins, P. E.; Huang, J.; Brinker, C. J.; Dravid, V. P. *Angew. Chem. Int. Ed.* **2013,** 52, 4160-4164.
(30) Liu, T.; Wang, C.; Gu, X.; Gong, H.; Cheng, L.; Shi, X.; Feng, L.; Sun, B.; Liu, Z. *Adv. Mater.* **2014,** 26, 3433-3440.
(31) Ai, K.; Ruan, C.; Shen, M.; Lu, L. *Adv. Funct. Mater.* **2016,** 5542–5549.
(32) Wang, H.; Yuan, H.; Hong, S. S.; Li, Y.; Cui, Y. *Chem. Soc. Rev.* **2015,** 44, 2664-2680.

(33) Li, H.; Wu, J.; Yin, Z.; Zhang, H. *Acc. Chem. Res.* **2014,** 47, 1067-1075.
(34) Wang, Z.; Mi, B. *Environ. Sci. Technol.* **2017,** 51, 8229-8244.
(35) Deng, M.; Kwac, K.; Li, M.; Jung, Y.; Park, H. G. *Nano Lett.* **2017,** 17, 2342–2348.
(36) Hirunpinyopas, W.; Prestat, E.; Worrall, S. D.; Haigh, S. J.; Dryfe, R. A.; Bissett, M. A. *ACS Nano* **2017,** in press.
(37) Qiu, L.; Zhang, X.; Yang, W.; Wang, Y.; Simon, G. P.; Li, D. *Chem. Commun.* **2011,** 47, 5810-5812.
(38) Benck, J. D.; Lee, S. C.; Fong, K. D.; Kibsgaard, J.; Sinclair, R.; Jaramillo, T. F. *Adv. Energy Mater.* **2014,** 4, 1400739.
(39) Britto, R. J.; Benck, J. D.; Young, J. L.; Hahn, C.; Deutsch, T. G.; Jaramillo, T. F. *J. Phys. Chem. Lett.* **2016,** 7, 2044-2049.
(40) Eda, G.; Yamaguchi, H.; Voiry, D.; Fujita, T.; Chen, M.; Chhowalla, M. *Nano Lett.* **2011,** 11, 5111-5116.
(41) Wang, Z.; von dem Bussche, A.; Qiu, Y.; Valentin, T. M.; Gion, K.; Kane, A. B.; Hurt, R. H. *Environ. Sci. Technol.* **2016,** 50, 7208–7217.
(42) Heising, J.; Kanatzidis, M. G. *J. Am. Chem. Soc.* **1999,** 121, 11720-11732.
(43) Hansen, E. L.; Hemmen, H.; Fonseca, D. d. M.; Coutant, C.; Knudsen, K.; Plivelic, T.; Bonn, D.; Fossum, J. O. *Sci. Rep.* **2012,** 2, 618.
(44) Hodge, R.; Edward, G. H.; Simon, G. P. *Polymer* **1996,** 37, 1371-1376.
(45) Li, D.; Müller, M. B.; Gilje, S.; Kaner, R. B.; Wallace, G. G. *Nat. Nanotechnol.* **2008,** 3, 101-105.
(46) Yotsumoto, H.; Yoon, R.-H. *J. Colloid Interface Sci.* **1993,** 157, 434-441.
(47) Leite, F. L.; Bueno, C. C.; Da Róz, A. L.; Ziemath, E. C.; Oliveira, O. N. *Int. J. Mol. Sci.* **2012,** 13, 12773-12856.
(48) Lu, C.-P.; Li, G.; Watanabe, K.; Taniguchi, T.; Andrei, E. Y. *Phys. Rev. Lett.* **2014,** 113, 156804.
(49) Salomão, F. C.; Lanzoni, E. M.; Costa, C. A.; Deneke, C.; Barros, E. B. *Langmuir* **2015,** 31, 11339-11343.
(50) Aba, N. F. D.; Chong, J. Y.; Wang, B.; Mattevi, C.; Li, K. *J. Membr. Sci.* **2015,** 484, 87-94.
(51) Choi, W.; Choi, J.; Bang, J.; Lee, J.-H. *ACS Appl. Mater. Interfaces* **2013,** 5, 12510-12519.
(52) Gao, S. J.; Qin, H.; Liu, P.; Jin, J. *J. Mater. Chem. A* **2015,** 3, 6649-6654.
(53) Han, Y.; Jiang, Y.; Gao, C. *ACS Appl. Mater. Interfaces* **2015,** 7, 8147-8155.
(54) Hu, M.; Mi, B. *J. Membr. Sci.* **2014,** 469, 80-87.
(55) Song, J. J.; Huang, Y.; Nam, S.-W.; Yu, M.; Heo, J.; Her, N.; Flora, J. R.; Yoon, Y. *Sep. Purif. Technol.* **2015,** 144, 162-167.
(56) Wang, L.; Wang, N.; Li, J.; Li, J.; Bian, W.; Ji, S. *Sep. Purif. Technol.* **2016,** 160, 123-131.
(57) Wang, W.; Eftekhari, E.; Zhu, G.; Zhang, X.; Yan, Z.; Li, Q. *Chem. Commun.* **2014,** 50, 13089-13092.
(58) Xia, S.; Ni, M.; Zhu, T.; Zhao, Y.; Li, N. *Desalination* **2015,** 371, 78-87.
(59) Zhang, Y.; Zhang, S.; Chung, T.-S. *Environ. Sci. Technol.* **2015,** 49, 10235-10242.
(60) Zhang, Y.; Zhang, S.; Gao, J.; Chung, T.-S. *J. Membr. Sci.* **2016,** 515, 230-237.
(61) Algara-Siller, G.; Lehtinen, O.; Wang, F.; Nair, R.; Kaiser, U.; Wu, H.; Geim, A.; Grigorieva, I. *Nature* **2015,** 519, 443-445.
(62) Maniwa, Y.; Kataura, H.; Abe, M.; Udaka, A.; Suzuki, S.; Achiba, Y.; Kira, H.; Matsuda, K.; Kadowaki, H.; Okabe, Y. *Chem. Phys. Lett.* **2005,** 401, 534-538.
(63) Kwac, K.; Kim, I.; Pascal, T. A.; Goddard III, W. A.; Park, H. G.; Jung, Y. *J. Phys. Chem. C* **2017**.

(64) Barrowman, J. A., *Physiology of the gastro-intestinal lymphatic system*. CUP Archive: 1978.
(65) Gendron, P.-O.; Avaltroni, F.; Wilkinson, K. *J. Fluoresc.* **2008,** 18, 1093.
(66) Hummers Jr, W. S.; Offeman, R. E. *J. Am. Chem. Soc.* **1958,** 80, 1339-1339.
(67) Marcano, D. C.; Kosynkin, D. V.; Berlin, J. M.; Sinitskii, A.; Sun, Z.; Slesarev, A.; Alemany, L. B.; Lu, W.; Tour, J. M. *ACS Nano* **2010,** 4, 4806-4814.
(68) Zheng, S.; Tu, Q.; Urban, J. J.; Li, S.; Mi, B. *ACS Nano* **2017,** 11 6440–6450.
(69) Voinova, M. V.; Rodahl, M.; Jonson, M.; Kasemo, B. *Phys. Scr.* **1999,** 59, 391.
(70) Berendsen, H. J.; van der Spoel, D.; van Drunen, R. *Comput. Phys. Commun.* **1995,** 91, 43-56.
(71) Van Der Spoel, D.; Lindahl, E.; Hess, B.; Groenhof, G.; Mark, A. E.; Berendsen, H. J. *J. Comput. Chem.* **2005,** 26, 1701-1718.
(72) Humphrey, W.; Dalke, A.; Schulten, K. *J. Mol. Graphics* **1996,** 14, 33-38.
(73) Jorgensen, W. L.; Tirado-Rives, J. *J. Am. Chem. Soc.* **1988,** 110, 1657-1666.
(74) Berendsen, H.; Grigera, J.; Straatsma, T. *J. Phys. Chem.* **1987,** 91, 6269-6271.
(75) Nosé, S. *J. Chem. Phys.* **1984,** 81, 511-519.
(76) Hoover, W. G.; Hoover, C. *Condens. Matter Phys.* **2005,** 8, 42.

For TOC only

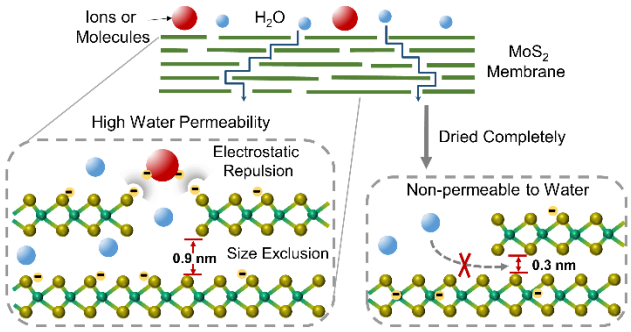
Ions or Molecules
H_2O
MoS_2 Membrane
High Water Permeability
Electrostatic Repulsion
0.9 nm
Size Exclusion
Dried Completely
Non-permeable to Water
0.3 nm